Unravelling the Active Vanadium Sites and Adsorbate Dynamics in VO_x/CeO_2 Oxidation Catalysts Using Transient IR Spectroscopy

Leon Schumacher, Jakob Weyel, Christian Hess*

Eduard Zintl Institute of Inorganic and Physical Chemistry, Technical University of Darmstadt, Alarich-Weiss-Str. 8, 64287 Darmstadt, Germany

*Corresponding Author (E-Mail: christian.hess@tu-darmstadt.de)

Abstract

The oxidative dehydrogenation (ODH) of propane over supported vanadia catalysts is an attractive route towards propene (propylene) with the potential of industrial application and has been extensively studied over decades. Despite numerous mechanistic studies, the active vanadyl site of the reaction has not been elucidated. In this work, we unravel the ODH reaction mechanism, including the nuclearity-dependent vanadyl and surface dynamics, over ceria-supported vanadia (VO_x/CeO_2) catalysts by applying (isotopic) modulation excitation IR spectroscopy supported by *operando* Raman and UV-Vis spectroscopies. Based on our loading-dependent analysis, we were able to identify two different mechanisms leading to propylene, which are characterized by isopropyl- and acrylate-like intermediates. The modulation excitation IR approach also allows for the determination of the time evolution of the vanadia, hydroxyl, and adsorbate dynamics, underlining the intimate interplay between the surface vanadia species and the ceria support. Our results highlight the potential of transient IR spectroscopy to provide a detailed understanding of reaction mechanisms in oxidation catalysis and the dynamics of surface catalytic processes in general.

TOC Graphic

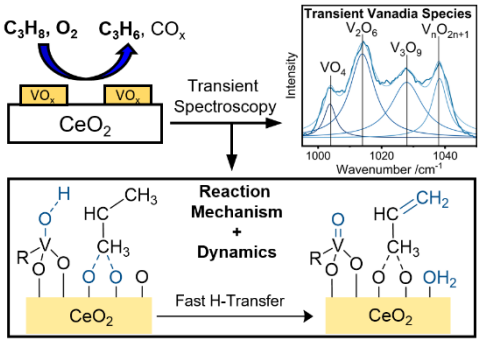

Keywords: oxidative dehydrogenation (ODH), propane, vanadia, ceria, transient spectroscopy, *operando* spectroscopy, modulation excitation spectroscopy

1. Introduction

Propylene (propene) is among the most important starting materials of the petrochemical industry and used for a variety of products. As the gap between demand and supply is constantly growing, alternative ways of producing propylene are of great interest. One such way is oxidative dehydrogenation (ODH), which shows favorable reaction characteristics in comparison to conventional processes such as steam cracking or fluid catalytic cracking.[1,2] Propane ODH is possible at lower temperatures and is exothermic in nature, thereby reducing energy expenditure, while the addition of oxygen to the reaction feed decreases catalyst deactivation due to coke formation or leaching.[3] However, it has been a challenge to find active and highly selective catalysts to avoid over-oxidation to CO_x.[4]

For a rational design of better catalysts, a detailed understanding of the mode of operation and identification of the active sites are crucial but remain a tremendous challenge. Despite the extensive success of applying *in situ/operando* approaches to catalysts under steady-state conditions,[5] access to the reaction dynamics requires the use of transient spectroscopy, for example modulation excitation spectroscopy (MES), which changes one parameter (typically the concentration) over time and measures the system's response.[6] In fact, besides significant noise reduction, such an approach allows discrimination between active and spectator species, and thus a focus on the crucial aspects of the mechanism. In heterogeneous catalysis, MES has been mostly used to study reactions of small molecules, e.g., CO oxidation,[7–14] NH_3-SCR (selective catalytic reduction),[15–17] and CO_2 activation,[18–21] but to the best of our knowledge there has been no application in the context of the economically important field of alkane oxidation catalysis.

As suitable catalysts for ODH of short alkanes, especially propane, mainly vanadia but also NiO- and boron oxide–based catalysts have been discussed.[3,22,23] In particular, catalysts with amorphous surface vanadia species (VO_x) as the active phase have shown promising performances during propane ODH, but further catalyst optimization is still required.[3,24–29] Besides the active phase, the choice of the support material is of great importance and has been proposed to increase the catalytic performance in the case of active support materials such as CeO_2 and TiO_2 due to their direct participation in the reaction.[3,25,29] Recently, ceria-supported vanadia (VO_x/CeO_2) catalysts have attracted increased attention, both theoretically[30–34] and

experimentally.[3,25,26,29,35–38] Nevertheless, direct experimental insight into the reaction intermediates and the surface dynamics have not been reported yet.

Previous theoretical studies focused on general properties of VO_x/CeO_2 catalysts and concluded that the participation of ceria in oxidation reactions is related to its low defect formation energy,[30,32,33] keeping vanadium in the oxidation state V^{5+}.[34–37,39] Density functional theory (DFT) calculations on propane ODH have proposed multiple pathways towards propylene but were not conclusive due to their small energy differences.[33] Experimental studies using Raman spectroscopy have demonstrated the interaction of vanadia with ceria oxygen vacancies,[40] which was supported by DFT calculations,[32] and later by X-ray absorption near-edge structure spectroscopy (XANES) in the context of ethane ODH.[35] Our previous work[27] confirmed the active participation of ceria in the oxidation process and also the structural relaxation of monomeric vanadia sites into surface oxygen vacancies, irreversibly blocking them for propane ODH.

One of the major open questions in oxidation catalysis over supported vanadia catalysts has been the influence of vanadia nuclearity on catalytic performance and the involvement of vanadyl groups in the reaction mechanism. In this mechanistic study, we address these vanadia-related aspects besides the surface and adsorbate dynamics during the ODH of propane over VO_x/CeO_2 catalysts using transient IR spectroscopy supported by steady-state *operando* spectroscopies (diffuse reflectance infrared Fourier transform spectroscopy (DRIFTS), Raman, UV-Vis). We highlight the potential of (isotopic) modulation excitation IR spectroscopy to add crucial new information to the mechanistic understanding of oxidation catalysts, thus greatly facilitating their rational design.

2. Experimental Section

2.1. Catalyst Preparation

The ceria support was prepared as previously described[41] and loaded with vanadia by incipient wetness impregnation. Three different loadings were prepared by mixing 1 g of ceria with 0.5 mL of different-concentration precursor solutions (1.07 mol/L, 0.51 mol/L, and 0.21 mol/L) containing vanadium(V) oxytriisopropoxide (≥97%, Sigma Aldrich) and 2-propanol (99.5%, Sigma Aldrich). The samples were then heated to 600 °C at a heating rate of 1.5 C/min and calcined for 12 h. The specific surface area of bare ceria was determined to be 61.4 m²/g by nitrogen physisorption experiments and the use of the Brunauer–Emmett–Teller (BET) method, yielding vanadium loadings of 2.83 V/nm² (2.32 wt% V_2O_5), 1.36 V/nm² (1.11 wt% V_2O_5), and 0.57 V/nm² (0.47 wt% V_2O_5), respectively. Higher vanadium loadings were not considered since vanadia crystallites were shown to be present at loadings >2.9 V/nm².[42] The resulting catalyst powders were subsequently pressed at a pressure of 2000 kg/m² for 20 s, ground and then sieved using a combination of sieves to obtain 200–300 µm particles.

2.2. X-Ray Diffraction

Powder X-ray diffraction (XRD) patterns were recorded on a Stoe Stadi P diffractometer with a Ge(111)-monochromator, Cu Kα radiation (λ = 1.54060 Å), and a MYTHEN-1K Dectris detector, using a flat sample holder in transmission geometry. The powder XRD patterns were recorded after the synthesis of the samples.

2.3. UV-Raman Spectroscopy

UV-Raman spectroscopy was performed at an excitation wavelength of 385 nm generated by a laser system based on a Ti:Sa solid state laser pumped by a frequency-doubled Nd:YAG laser (Coherent, Indigo). The fundamental wavelength is frequency doubled to 385 nm using a LiB_3O_5 crystal. The light is focused onto the sample, and the scattered light is collected by a confocal mirror setup and focused into a triple-stage spectrometer (Princeton Instruments, TriVista 555).[42] Finally, the Raman contribution is detected by a charge-coupled device (CCD, 2048 × 512 pixels) cooled to –120 °C. The spectral resolution of the spectrometer is 1 cm^{-1}. For Raman experiments, 70 mg of catalyst was placed in a CCR 1000 reactor (Linkam Scientific Instruments) equipped with a CaF_2 window (Korth Kristalle GmbH). A fluidized bed reactor was employed to avoid laser-induced damage, allowing the use of a laser power of 9 mW at the location

of the sample. Data processing included cosmic ray removal and background subtraction. For structural characterization, spectra were measured at room temperature after dehydration at 366 °C in 12.5% O_2/He for 1 h. *Operando* spectra were measured at 275 °C during exposure to reactive conditions (12.5% C_3H_8/12.5% O_2/He) in comparison to oxidizing conditions (12.5% O_2/He) after 1 h of dehydration in 12.5% O_2/He at 366 °C with a total flow rate of 40 ml_n/min. The spectra were further analyzed by a least-squares fitting analysis using Lorentzian functions.

2.4. Visible Raman Spectroscopy

Visible (Vis) Raman spectroscopy was performed at 514 nm excitation, emitted from an argon ion gas laser (Melles Griot). The light was focused onto the sample, gathered by an optical fiber and dispersed by a transmission spectrometer (Kaiser Optical, HL5R). The dispersed Raman radiation was subsequently detected by an electronically cooled CCD detector (–40 °C, 1024 × 256 pixels). The spectral resolution was 5 cm^{-1} with a wavelength stability of better than 0.5 cm^{-1}. For Raman experiments, 70 mg of catalyst was filled into a CCR 1000 reactor (Linkam Scientific Instruments) equipped with a quartz window (Linkam Scientific Instruments). The laser power at the sample location was 2.5 mW. Data analysis of the Raman spectra included cosmic ray removal and an auto new dark correction. For structural characterization, spectra were measured at room temperature after dehydration at 366 °C in 12.5% O_2/He for 1 h. *Operando* spectra were measured at 275 °C during exposure to 12.5% C_3H_8/12.5% O_2/He), in comparison to oxidizing conditions (12.5% O_2/He), after 1 h of dehydration in 12.5% O_2/He at 366 °C with a total flow rate of 40 ml_n/min. The vanadyl region was fit using Lorentzian functions at distinct spectral positions representative of the different vanadia nuclearities with a fluctuation of 1 cm^{-1}. The F_{2g} mode was fitted without any positional restrictions due to the possible occurrence of red-shifts.

2.5. Diffuse Reflectance UV-Vis Spectroscopy

Diffuse reflectance (DR) UV-Vis spectra were recorded on a Jasco V-770 UV-Vis spectrometer. Dehydrated $BaSO_4$ was used as the white standard. For each experiment, 90 mg of catalyst was put in the commercially available reaction cell (Praying Mantis High Temperature Reaction Chamber, Harrick Scientific) equipped with transparent quartz glass windows. For structural characterization, spectra were measured at room temperature after dehydration at 366 °C in 12.5% O_2/He for 1 h. *Operando* spectra were measured at 275 °C during exposure to 12.5% C_3H_8/12.5%

O_2/He), in comparison to oxidizing conditions (12.5% O_2/He), after 1 h of dehydration in 12.5% O_2/He at 366 °C with a total flow rate of 40 ml_n/min.

2.6. Catalytic Measurements

Catalytic testing was performed in a CCR 1000 reaction cell in a fluidized bed using 90 mg of catalyst. The sample was first dehydrated for 1 h at 366 °C in 12.5% O_2/He. The catalyst was then cooled to 50 °C, exposed to 12.5% O_2/12.5% C_3H_8/He with a total flow rate of 40 ml_n/min, and heated in 45 °C steps up to 500 °C, staying at each temperature for 1 h. The gas-phase composition was analyzed continuously using gas chromatography (GC, Agilent Technologies 7890B). The GC is equipped with a PoraPlotQ and a Molsieve column as well as a thermal conductivity detector (TCD) and a flame ionization detector (FID) in series. The setup is connected through a twelve-way valve. One chromatogram is measured every 29 min, resulting in two chromatograms for each temperature, which were averaged. The pressure before and after the GC was monitored to correct the detected areas for pressure fluctuations.

2.7. DRIFTS

DRIFT spectra were recorded on a Vertex 70 spectrometer (Bruker), equipped with a liquid nitrogen–cooled mercury cadmium telluride (MCT) detector, operating at a resolution of 1 cm^{-1}. Dehydrated potassium bromide was used as an infrared transparent sample for the background spectrum. For each experiment, 90 mg of the catalyst was placed in the reaction cell (Praying Mantis High Temperature Reaction Chamber, Harrick Scientific) equipped with transparent KBr windows. The sample was dehydrated for 1 h in 12.5% O_2/He at 366 °C, cooled to 50 °C, and then exposed to 12.5% O_2/12.5% C_3H_8/He. After 30 min of equilibration, a spectrum was recorded. The sample was then heated in 45 °C steps to 320 °C and DRIFT spectra were recorded after 30 min at each temperature. In all measurements, the total flow rate was set to 40 ml_n/min.

Data processing consisted of background removal by subtraction of a baseline formed by 12 anchor points. A background spectrum of the gas-phase was recorded using KBr as an infrared transparent sample. The propane gas-phase and the *operando* spectra were then normalized to the propane gas-phase peak at ~3000 cm^{-1} and subtracted to remove propane gas-phase contributions. Example data processing for ceria loaded with 0.57 V/nm² is shown in Fig. S1.

2.8. Modulation Excitation (ME)-DRIFTS

ME-DRIFT spectroscopy was performed using the same apparatus as for steady-state DRIFTS; a more detailed description of our basic DRIFTS setup and the modifications made for recording ME-DRIFT spectra (see Fig. S2) have already been published.[14,43,44,45] For each experiment, 90 mg of catalyst was used.

We used the rapid scan mode extension of Bruker's spectrometer software OPUS 7.2. Spectra were measured from 850 to 3800 cm^{-1} with a resolution of 0.5 cm^{-1}, an aperture of 8 mm, and a mirror speed of 40 kHz. A Valco Instruments 4/2 valve (Model E2CA, version ED), communicating with the Vertex 70, is used to rapidly switch between different gas feeds, which are controlled *via* digital mass flow controllers (Bronkhorst).

As gases we used C_3H_8 (Westfalen, 3.5), C_3D_8 (Eurisotope, 98% isotopic labeling), O_2 (Westfalen, 5.0), and helium (Westfalen, 5.0). One measurement series consisted of 20 periods (20 gas-phase switches), each of which had a duration of 360 s and consisted of 240 spectra. For one spectrum, five consecutive interferograms were averaged, so that a new spectrum was acquired every 1.54 s.

As background the catalyst spectrum itself was used, after 60 min of dehydration at 366 °C in 12.5% O_2/helium atmosphere and a 10 min treatment at 275 °C in one of the reaction gases for conventional ME-DRIFTS (12.5% O_2 or 12.5% C_3H_8 in helium) or in reaction gas atmosphere (12.5% C_3H_8/12.5% O_2/75% He) for isotope ME-DRIFTS. The flow was kept constant at 100 mL_n/min during the pretreatment and experiment.

During conventional ME-DRIFTS, a flow of either 12.5% C_3H_8 or 12.5% O_2 in helium was kept constant over the sample, while the other feed gas was pulsed over the sample. In our isotope ME-DRIFTS experiments, the propane-h8-containing reaction atmosphere was switched to a propane-d8-containing reaction atmosphere, while the flow of oxygen through the reaction chamber was constant.

The temperature during all modulation excitation experiments was kept at 275 °C. To remove the gas-phase contribution, we subtracted gas-phase spectra over KBr (see Fig. S3) from each recorded DRIFT spectrum. To exclude the possibility of intensity fluctuations over multiple periods, we checked the intensity profile at three distinct wavenumbers, representative of the background, an adsorbate peak, and a gas-phase peak, but detected no absolute intensity changes over multiple periods that could influence the Fourier transformation (see Fig. S4). Peak-fitting analysis of ME-DRIFT spectra was performed using Lorentzian functions employing the Levenberg–Marquardt algorithm implemented in OriginLab 2018.

To obtain phase-sensitive spectra, the time-resolved 3D spectral data was converted from the time to the phase domain. For an overview, the resolution of phase spectra was chosen to be 30°, whereas mechanistic insights were obtained using a resolution of 1°. The main operation of phase-sensitive detection (PSD) is a Fourier transformation according to[46]

$$I_{\tilde{\nu}}(\varphi) = \frac{2}{T}\int_{0}^{T} I_{\tilde{\nu}}(t) \cdot \sin(2\pi f t + \varphi)\, dt$$

where $I(t)$ is the time-dependent intensity at one specified wavenumber ($\tilde{\nu}$) that is convoluted with the sine function, representing the modulation of the external parameter (e.g., the gas-phase concentration), thus forming $I(\varphi)$, the phase-resolved intensity. The frequency of the external modulation is f, whereas 0 and T represent the times at which the considered dataset begins and ends, respectively. To obtain a complete phase-resolved spectrum, this procedure is repeated for every wavenumber. By varying φ from 0 to 360° with a chosen resolution and repeating the steps above, the complete phase-resolved dataset is created.

To obtain time constants for a particular wavenumber, first the phase angle in the PSD function is determined where $I(t)$ shows the best overlap with the external modulation function. This is done for a set of chosen peak positions. To this end, the phase angle corresponding to the phase spectrum with the largest signal at the particular wavenumber is extracted by automatically comparing the intensities for spectra of all the different phase angles. The following equation is used to translate this phase angle back into a time value within the interval of one period, in order to make it more interpretable:

$$t_{con} = \frac{(360 - \varphi_{\mathbf{max}})}{360} \cdot t_{\mathbf{per}}$$

The experimental error is 1.54 s, which represents the measurement time of one spectrum. Regarding the temporal analysis of the vanadyl peak, the time constants of the overtones were considered due to their much higher accuracy in comparison to the fundamental vibration. A detailed description and discussion of this effect is given in the supporting information (see Fig. S5 and the attached discussion). Further details regarding the used software and the full code, which is available free of charge at GitHub, can be found elsewhere.[47]

3. Results and Discussion

3.1. Catalytic Activity and *Operando* Spectroscopy

The structure of the synthesized VO_x/CeO_2 catalysts was characterized using XRD, UV-Vis, and Raman spectroscopy, confirming the presence of polycrystalline ceria and amorphous surface vanadia at all loadings (see Fig. 1). Even at the highest loading, there is no indication of crystalline V_2O_5 (Raman, Fig. 1c) or $CeVO_4$ (XRD, Fig. 1a).[48] Detailed assignments for XRD, UV-Vis, and Vis-Raman bands are given elsewhere.[27] Besides the ceria and the interface-related Raman features discussed below, the vanadyl (V=O) stretching region is resolved especially well at 514 nm excitation[49] and is characterized by nuclearity-dependent features at 1008, 1015, 1023, 1032, and 1040 cm^{-1}, which are attributed to monomeric, dimeric, trimeric, tetrameric, and pentameric species, respectively (see inset of Fig. 1c).[40,50] The loading-dependent nuclearity distribution resulting from a peak-fit analysis, depicted in Fig. S6, shows a shift in in the maximum of the distribution from dimeric to trimeric species at higher vanadium loadings.

Figure 2 summarizes results from the temperature- and loading-dependent *operando* analysis of VO_x/CeO_2 catalysts during propane ODH, using *operando* DRIFT, UV-Vis, and Raman spectroscopies. Figure 2a depicts the temperature-dependent propane conversions in 12.5 % O_2/ 12.5 % C_3H_8 /He, in comparison to bare ceria. The empty reaction cell has no significant influence on the activity data (conversion <0.1 %).[27] The onset of conversion is located at 230 °C for all catalysts and reaches a plateau at around 450 °C. For the following discussion, a temperature of 275 °C was chosen (dashed line), at which gas-phase processes can be excluded and conversions are <15% (differential conditions). Besides, propylene selectivities are maximized to ensure the investigation of the selective oxidation pathway rather than total oxidation. Figure 2b shows the loading-dependent conversions and selectivities at 275 °C (for details, please refer to Fig. S7). Even small amounts of vanadia (0.57 V/nm^2) strongly affect the propylene selectivity, but for further additions of vanadia the increase in selectivity becomes increasingly smaller. Due to the different conversions and selectivities, the oxygen consumption of the catalysts is different and therefore the oxygen partial pressure may change differently for the samples. To exclude any significant effects of the different oxygen partial pressures on our observed activities and structural dynamics, the oxygen concentrations and the corresponding propylene

selectivities for all samples during propane ODH at 275 ° are given in Figure S8. The differences in oxygen concentration for all vanadia-loaded samples are very similar and a change in vanadium oxidation state due to this small difference appears unlikely. In comparison, the decrease in gas-phase oxygen due to the very high CO_2 production of ceria deviates significantly from the vanadia-loaded samples. As ceria takes 75 minutes to reach an equilibrium oxygen concentration and the selectivity changes are in the same time frame, it can be assumed that the changes in oxygen concentration from an initial 45% up to a 75% decrease in oxygen concentration correspond to those observed for the propylene selectivity, i.e., a selectivity increase from 2.9 to 4.2%. This reveals a slight effect of the oxygen concentration on the reactivity behavior, which however is significantly lower than the influence of vanadium. In addition, while for ceria the amount of oxygen largely drops under reaction conditions, there is still enough oxygen present during equilibrium concentrations (after 200-250 minutes, 27% of initial oxygen) to not limit the conversion. Therefore, we can conclude that our measurements represent changes caused by vanadia (see below) and that the observed structural dynamics is not a result of different conversions. The catalytic data produced in our reaction cell is in good agreement with that from a fixed bed reactor at similar vanadium loadings and temperatures.[29]

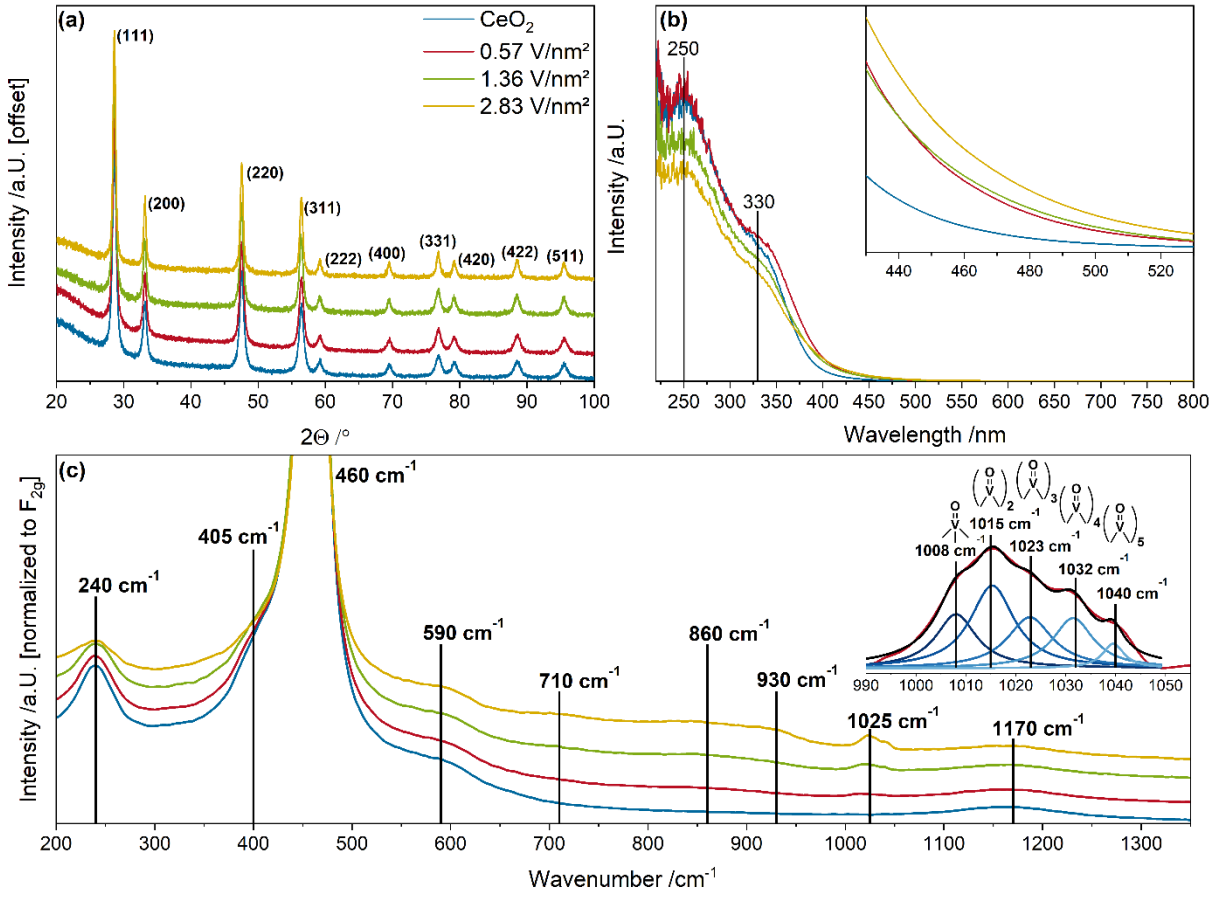

Figure 1: Summary of characterization data of VO_x/CeO_2 catalysts and bare ceria. **(a)** XRD diffraction patterns and **(b)** UV-Vis spectra. Diffraction peaks and absorption bands characteristic for CeO_2 are highlighted. For clarity, the region within 430–530 nm is enlarged. **(c)** Raman spectra at 514 nm excitation. The inset shows an example fit to the vanadyl signal of the 0.57 V/nm² sample with assigned structural features. All characterization data was measured after dehydration (12.5 % O_2/ He at 365 °C for 1 h).

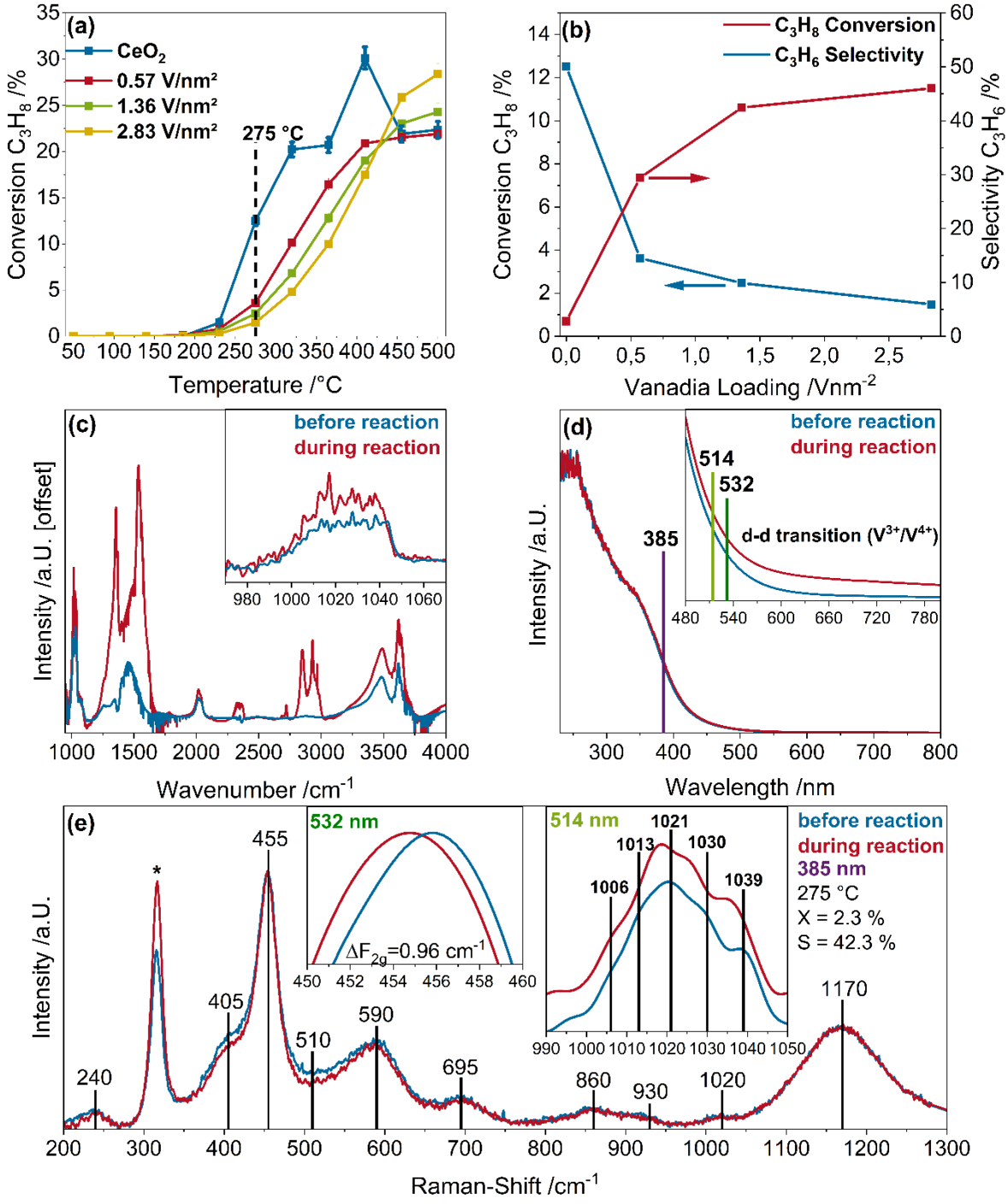

Figure 2: Results from the *operando* analysis of VO_x/CeO_2 catalysts during propane ODH. **(a)** Propane conversions compared to bare CeO_2 (with error bars). The dotted line marks the temperature of the *operando* experiments. **(b)** Loading-dependent propane conversions and propylene selectivities at 275 °C. **(c) – (e)** Exemplary *operando* spectroscopic results for the 1.36 V/nm² sample at 275 °C upon exposure to a feed of 12.5 % C_3H_8/ 12.5 % O_2/ He (red), compared to oxidative conditions, i.e., 12.5 % O_2/ He (blue). **(c)** DRIFT spectra with an enlarged view of the vanadyl region (inset). **(d)** UV-Vis spectra including the three excitation

wavelengths used for Raman spectroscopy. The inset shows the region of vanadia d-d transitions. **(e)** UV-Raman spectra at 385 nm laser excitation. The insets provide enlarged views of the vanadyl (514 nm) and F_{2g} (532 nm) regions.

As a basis for the transient spectra discussed below, Fig. 2c–e provides an overview of major results from the *operando* spectroscopic analysis at 275 °C, exemplarily shown for the 1.36 V/nm² sample for clarity (see Figs. S10–S13 for the other samples). Figure 2c depicts the *operando* DRIFT spectrum during propane ODH (red). In comparison to the spectrum obtained under oxidative conditions (blue), multiple new features and intensity changes are observed in the carbonate (1100–1800 cm^{-1}), C-H stretching (2700–3000 cm^{-1}), and hydroxyl (3500–3900 cm^{-1}) regions (see Table S1 for detailed assignments). The C-H stretch vibrations originate from propane that is adsorbed on the ceria surface.[51] The intensity changes of the hydroxyl groups at 3640, 3690, and 3740 cm^{-1} indicate hydrogen abstraction from propane to the ceria surface, either directly, i.e., without any involvement of surface vanadia species, or by rapid transfer from a vanadia species to the ceria surface. Especially the increase in intensity at 3740 cm^{-1} indicates the formation of an isopropylic state via hydrogen transfer from propane to ceria lattice oxygen.[52,53]

The dramatic changes in the carbonate region during reaction conditions result from the formation of adsorbates, which is related to the presence of propane in comparison to oxidative conditions. These include the appearance of a shoulder at 1610 cm^{-1}, originating from the propylene double bond, as well as the features at 1545 and 1567 cm^{-1}, which are usually assigned to O-C-O vibrations of carbonates and may be indicative of propane adsorption in an O-C-O geometry as well as subsequent CO_2 formation from carbonates (see Fig. S9 for detailed DRIFT spectra).[27,51,54,55] In this context it is important to note that the presented DRIFT spectra do not allow one to distinguish between spectator and mechanistically relevant (active) species. Finally, surface vanadia is detected via the V=O stretch vibration at 1020–1040 cm^{-1} and its overtone. However, as can be seen from the inset of Fig. 2c, no information about the nuclearity of the species and/or reaction-induced changes is revealed, due to the noise level in this region.

Fig. 2d shows the UV-Vis spectra recorded under oxidative (blue) and reactive (red) atmosphere. Generally, the UV-Vis spectra are characterized by the strong absorption of ceria below 400 nm caused by band gap absorption,[56] overlapping with ligand-to-

metal charge transfer (LMCT) features of vanadia between 300 and 550 nm.[57] Upon exposure to ODH conditions, multiple changes are detected. First, the observed absorption increase implies a red-shift of the band gap by 0.02 eV, which is indicative of ceria reduction in the ceria subsurface/bulk since newly created oxygen vacancies lead to electronic states closer to the conduction band, thereby decreasing the overall band gap.[41,58] Further changes in the absorption behavior at 550–800 nm (see inset of Fig. 2d) can be associated with vanadia d-d transitions, indicating the presence of reduced vanadia during reaction.[59,60] This is a remarkable observation as a number of experimental and theoretical studies have proposed that vanadia prefers an oxidation state of 5+ on the ceria surface.[30,32,34,35,37] In this context the question arises whether the reduction of vanadia species is an essential part of the reaction mechanism or a parallel process. Besides the gas-phase-induced changes, the spectra highlight the three Raman excitation wavelengths that have been chosen to allow for the most sensitive analysis of different parts of the catalyst system (385 nm: ceria surface; 514 nm: vanadia; 532 nm: ceria bulk), also exploiting resonance enhancements, as described previously.[26,27]

The corresponding *operando* Raman spectra are shown in Fig. 2e, in comparison to those recorded under oxidative conditions, all normalized to the F_{2g} mode. Exposure to ODH conditions leads to an intensity decrease of the Ce-O surface phonon at 405 cm^{-1} as well as the features within the range 470–600 cm^{-1} assigned to the defect region, containing a contribution of Ce^{3+} at 550 cm^{-1} and oxygen vacancies at 590 cm^{-1}.[41,44] This behavior indicates surface reduction of ceria, whereby lattice oxygen is used to oxidize propane to propylene and CO_x. Note that ceria, as an active support material, clearly participates in the reaction, in contrast to other carriers, such as SiO_2.[61,62] Interestingly, the vanadia structures (V-O-Ce, V-O-V, V=O) seem to remain unchanged during the reaction, as no observable intensity changes are detected between oxidative and reactive conditions, which is consistent with the previously mentioned literature but appears to be at odds with the d-d transitions observed in the UV-Vis spectra.

The UV-Raman behavior is supported by the 514 nm spectra, including the V=O profile (see inset of Fig. 2e, 514 nm), which shows a defined fine structure (see above), but remains largely unchanged, exhibiting a slight red-shift of the higher nuclearities but no clear trend when all four samples are considered (see Fig. S13). The F_{2g} mode is an important probe of the ceria subsurface/bulk properties. Using 532 nm excitation,

a red-shift of the F_{2g} mode of 0.96 cm^{-1} was detected when the gas atmosphere was switched to reactive conditions (see inset of Fig. 2e, 532 nm), which can be associated with ceria reduction, as the Ce^{3+} ions have a larger radius, leading to lattice expansion.[63] This is in good agreement with the band-gap shift deduced from the UV-Vis spectra, also indicating ceria reduction. From the above results, it is apparent that the ceria support actively participates in the reaction mechanism as an oxygen buffer, which provides surface oxygen for the ODH reaction and can be regenerated by either subsurface/bulk or gas-phase oxygen.

To gain further insight into the role of vanadia and to understand the significant activity changes of the catalyst upon vanadia impregnation, a quantitative analysis of the spectroscopic data was performed. The data is presented in Fig. S14 and summarizes the loading dependence of the dynamics of the transversal Ce-O surface phonon and the ceria defect region as well as the F_{2g} shift. Both trends are related to the oxygen dynamics within the ceria lattice. The Ce-O dynamics and the F_{2g} red-shift correlate with the observed conversions (see Fig. 2b), indicating that the reducibility of the catalyst is important for the conversion and that ceria supplies oxygen for the reaction. With increasing vanadium loading, the oxygen transfer towards the surface is slowed down, as also supported by the decreasing band gap energy shifts (see Fig. S14b). Considering the selectivity, the high oxygen dynamics in bare ceria counteract the selective oxidation to propylene and mostly CO_x is produced. From the above findings, we can deduce that the slowdown of the oxygen dynamics induced by surface vanadia species significantly increases the selectivity. The decrease in Raman intensity in the defect region correlates well with the amount of monomeric vanadia species in the samples (see Fig. S6), fully consistent with a DFT study by the Sauer group reporting a structural relaxation of monomeric vanadia species into newly created oxygen vacancies.[32] Therefore, as surface lattice oxygen is regarded as an active center for propane conversion leading to CO_x formation, as previously established,[64] this interaction leads to an overall slowdown of this reaction due to decreased oxygen mobility, thereby increasing the propylene selectivity. This explains the jump in propylene selectivity for 0.57 V/nm² and in part for 1.36 V/nm², but not for the highest vanadium loading with almost no monomeric species present. Thus, we suspect an additional reason for the selectivity increase at higher vanadium loadings, overlapping with the slowdown in oxygen dynamics induced by monomeric vanadia species.

3.2. Transient IR Spectroscopy

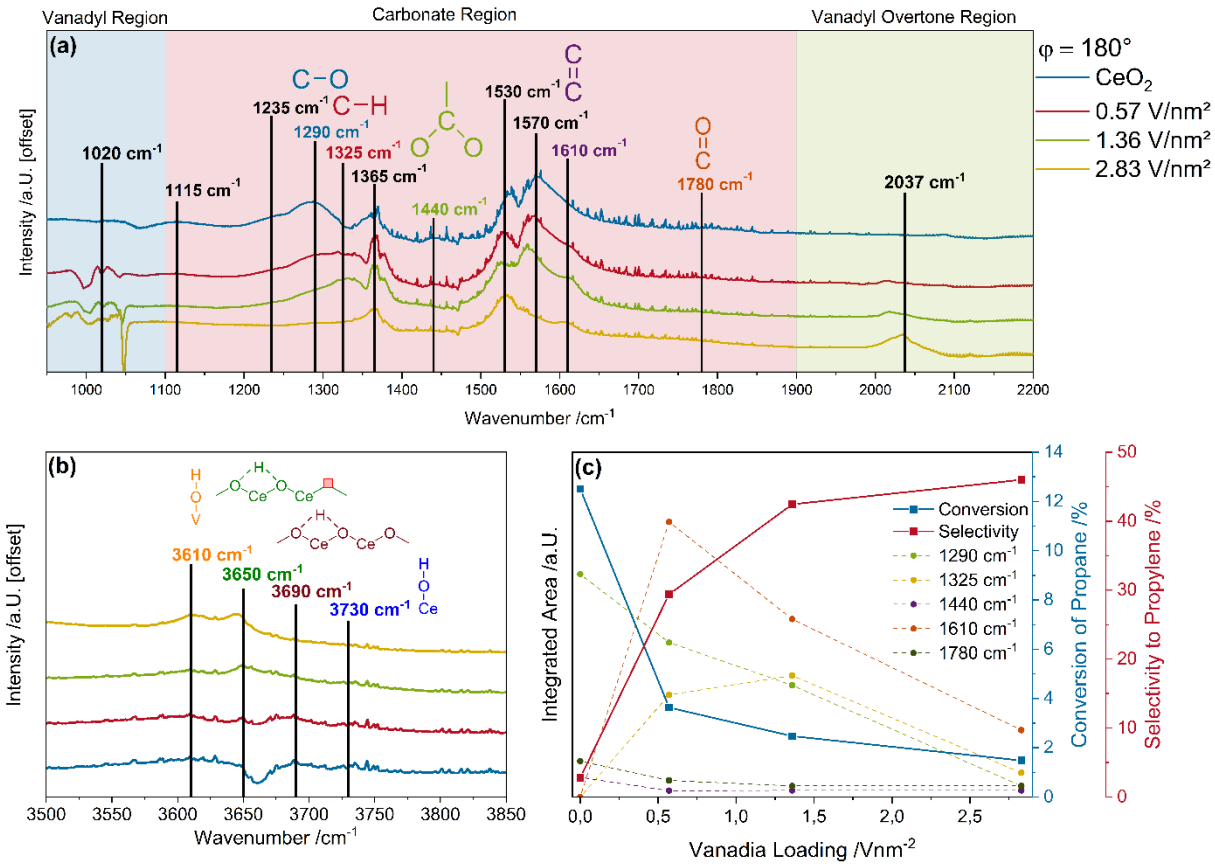

Figure 3: Results from transient IR spectroscopy for VO_x/CeO_2 catalysts compared to bare ceria during propane ODH at 275 °C. **(a)** PSD spectra (φ = 180°) at constant propane and pulsed oxygen flow highlighting adsorbate-related features of particular relevance for the mechanistic discussion. **(b)** PSD spectra of the Ce-OH region. **(c)** Loading-dependent peak areas of selected IR features related to the catalytic properties. An example fit of the spectrum of the 1.36 V/nm² sample is shown in the SI (see Fig. S19).

To further investigate the ODH reaction mechanism, we employed ME-DRIFTS, which is introduced in Figs. S15 a-e. The results of the measurements and the quantitative analysis are shown in Fig. 3. In the following discussion, we will focus on the spectra recorded in constant propane and pulsed oxygen at a phase shift of 180° (see Fig. 3a), at which the maximum intensities were detected. Corresponding spectra recorded in constant oxygen and pulsed propane show consistent results (see Figs. S16 and S18) but do not contain additional information, as discussed in detail in the SI (see Fig. S18). For clarity, in Fig. 3a the gas-phase contributions from CO, CO_2, and propane at 2100–3500 cm^{-1} have been removed and the relevant regions indicated. For the carbonate

region (center), detailed assignments and structures relevant for the quantitative analysis in Fig. 3c are depicted. The vanadyl regions (left and right) contain no detailed assignments at this point but will be discussed in detail below (see Figs. 4 and 5). Figure 3b highlights the Ce-OH region with its relevant structures. The peak assignments are summarized in Table 1.

Table 1: Peak assignments for the ME-DRIFT spectra of bare ceria and the vanadia-loaded samples recorded at 275 °C during constant propane and pulsed oxygen flow.

Position /cm^{-1}	Assignment	Reference
997	V=O monomeric	40,50
1004	V=O dimeric	40,50
1020	V=O trimeric	40,50
1040	V=O tetrameric	40,50
1049	V=O pentameric	40,50
1115	υ COO^-	55
1235	υ COO^-	55
1290	υ_s C-O	51
1325	υ C-H	65
1365	υ_s CH_3	51
1380	υ C-H	65
1440	υ_s COO	66
1530	υ_{as} COO	51
1570	υ_{as} COO	51
1610	υ_{as} C=C	51
1780	υ C=O	67
1994	V=O overtone	68
2017	V=O overtone	68
2037	V=O overtone	68
2087	V=O overtone	68
3610	V-O-H	69
3650	Ce-O-H II-B	70
3690	Ce-O-H II*-A	70
3730	Ce-O-H I-A	70

It is apparent that the transient spectra in Fig. 3a show smaller and more clearly defined peaks in the carbonate and hydroxyl region compared to Fig. 2c, underlining that some of the features in regular DRIFTS originate from spectator species. In addition, the presence of vanadyl peaks within 1000–1060 cm^{-1} as well as their overtones in the PSD spectra now evidence the active participation of the vanadyl group in the ODH reaction. Moreover, in contrast to Fig. 2c (inset), the vanadyl feature shows a clearly defined fine structure (see below), allowing a nuclearity-dependent analysis, which is of great importance considering the ongoing debate on the role of V=O in ODH reactions.[27,29,35,36,38] The participation of vanadia is also supported by the 3610 cm^{-1} peak in the OH stretching region, which is only detected for V-loaded samples, fully consistent with V-OH.[69] The Ce-OH peak located at 3730 cm^{-1}, which is commonly associated with an isopropylic adsorbate,[52,53] declines with increasing vanadium loading and is most pronounced for ceria, indicating that isopropyl adsorbate results from the first hydrogen abstraction from propane. The intensity decrease also correlates with the decrease in conversion, strongly suggesting that most, if not all, of the converted propane on ceria passes through an isopropyl adsorbate, as has been proposed in the literature.[51] The peaks at 3690 and 3650 cm^{-1} have been associated with bridged Ce-OH groups on clean ceria and located next to an oxygen vacancy, respectively.[41,70] With increasing vanadium loading, the 3650 cm^{-1} signal gains intensity while the 3690 cm^{-1} peak declines and is not observable anymore at higher loadings. This behavior highlights the importance of defects at higher vanadium loadings but also points to the relevance of other (V-related) surface processes besides the ceria oxygen dynamics discussed above, which is most pronounced at low loadings and becomes less relevant for higher loadings.

Owing to its significance for the interpretation of the ME-DRIFT spectra, a detailed analysis of the carbonate region was performed (see Fig. 3a). Species with significant intensity changes were analyzed quantitatively (dashed lines) and compared to the loading-dependent conversions and selectivities (solid lines). Starting with the region between 1200 and 1400 cm^{-1}, with increasing loading the features at 1235 and 1290 cm^{-1} decrease while the peak at 1325 cm^{-1} increases in relative intensity. The features at 1235 and 1290 cm^{-1} originate from adsorbates that contain C-O bonds,[51,55] which are likely to be strongly bound to the surface and, hence, to be over-oxidized to CO_x, decreasing the propylene selectivity. The peak at 1325 cm^{-1} is attributed to a C-H bond from a single hydrogen bound to carbon,[65] which is only possible at the middle

carbon atom of propane after double bond formation. Therefore, the presence of this peak is associated with selective oxidation to propylene rather than total oxidation.[65] The 0.57 V/nm² sample shows all three peaks, indicating that at low vanadium loadings both reaction pathways appear simultaneously. Besides, the feature at 1440 cm^{-1}, associated with an O-C-O containing adsorbate,[51,66] shows a decrease in intensity with increasing vanadium loading, representing the state in which the propane adsorbs to the catalyst surface, as can be verified by in-phase angle analysis (see below).

At higher wavenumbers, the peaks at 1610 and 1780 cm^{-1} are of interest, which originate from C=C and C=O stretching modes, respectively. The latter feature has been associated with CO_2 formation on MnO_x-ceria catalysts,[52] whereas the 1610 cm^{-1} peak, which increases with vanadium loading, was previously identified as part of an acrylate-based state in the context of Ru/CeO_2 catalysts used for propane combustion.[51] Therefore, the above findings suggest the presence of two different pathways towards propylene formation. One operates on the bare ceria and is based on an isopropyl transition state, as indicated by the presence of the corresponding Ce-OH groups, while the other one is based on an acrylic transition state, as evidenced by the C=C peak at 1610 cm^{-1}, and is formed by participation of vanadia.

These scenarios are corroborated by the loading-dependent correlations of structure with activity/selectivity in Fig. 3c. First, the peaks at 1290 and 1780 cm^{-1}, associated with adsorbates related to CO_x formation, follow the trend of the conversion, which is in line with the Raman results on the decreased oxygen dynamics (see above), as does the peak at 1440 cm^{-1}, associated with the initial adsorbate after the first hydrogen abstraction. As the first hydrogen abstraction is considered the rate-determining step of the ODH reaction, less adsorbed propane would lead to smaller conversions. Finally, the features at 1325 and 1610 cm^{-1}, related to propylene formation, show trends that at first sight appear to correlate with neither the conversion nor the selectivity. This is because catalysts with higher vanadium loadings have lower conversions, while the propylene yield stays almost constant. Therefore, the peak intensities at 1325 and 1610 cm^{-1} need to be regarded in relation to other peak intensities, such as those at 1290 and 1780 cm^{-1}. Indeed, for these relative intensities, a similar loading dependence as for the selectivities is observed.

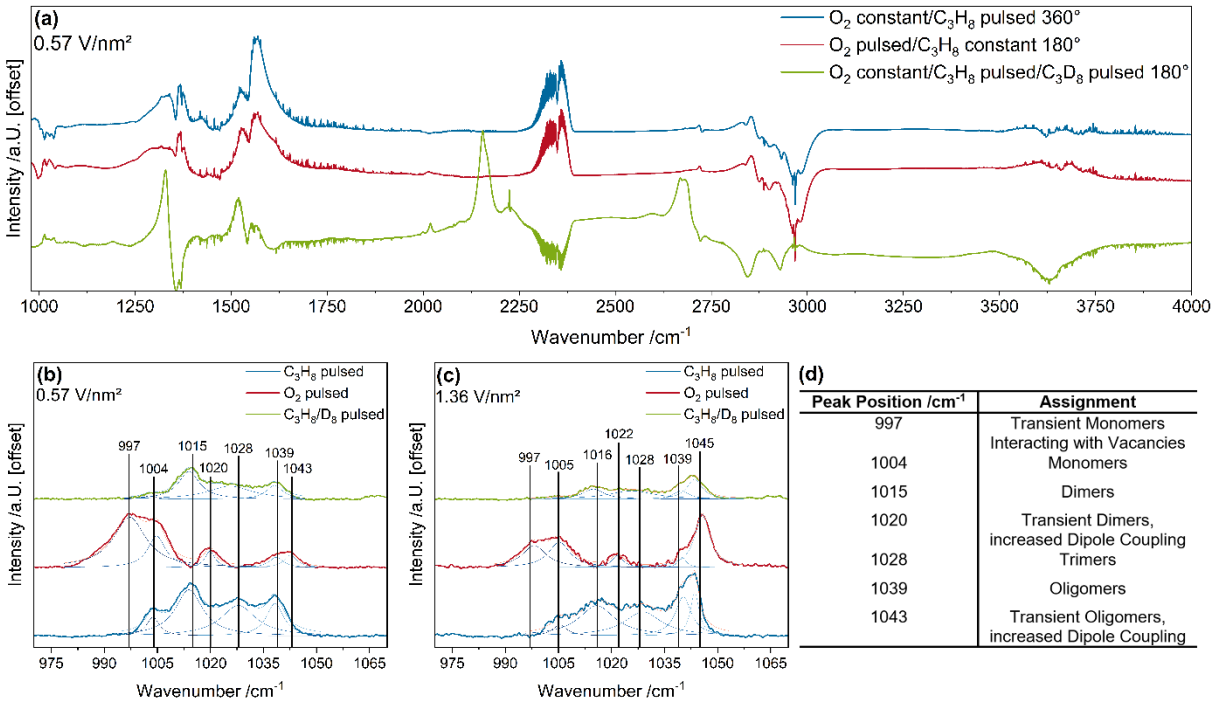

Figure 4: Results from isotopic transient IR spectroscopy during propane ODH at 275 °C. **(a)** PSD spectra during different ME-DRIFTS experiments. **(b-c)** Enlarged view of the vanadyl region for two different loadings, together with the result of a fit analysis. **(d)** Proposed assignments for the different vanadyl (V=O) signals during MES experiments. Please refer to the text for details and to Fig. S22 for MES results on the 2.83 V/nm² sample.

For further insight into the dynamics, we performed isotopic exchange experiments in which the propane-h8-containing reaction atmosphere was switched to a propane-d8-containing reaction atmosphere, while the flow of oxygen through the reaction chamber was constant. This experiment allows features to be identified that are associated with a hydrogen transfer during the reaction mechanism, as the only way of introducing hydrogen/deuterium is through propane. Figure 4a depicts an example spectrum for the 0.57 V/nm² catalyst, together with the results from the two modulation settings used above, while the spectra of the other samples are discussed in the SI (see Figs. S20 and S21). The results largely confirm those obtained for the OH and carbonate regions (see Fig. 3a). In the carbonate region, besides the major peaks at 1325 and 1360 cm^{-1}, small contributions due to COO modes are detected at 1440 and 1530 cm^{-1}, which are attributed to a kinetic isotope effect, showing its relevance for the first hydrogen abstraction to the catalyst's surface. Remarkably, the isotopic ME-DRIFT spectra provide important new insight into the vanadia dynamics, which goes beyond the *operando* Raman and DRIFTS results shown in Fig. 2. In fact, closer

inspection of the vanadyl region reveals a gas-phase-dependent fine structure, which is shown in an enlarged view in Fig.4 b-c together with results of a fit analysis. Figure 4d summarizes the proposed assignments for the transient vanadyl features.

Considering the (static) Raman results, the active participation of vanadyl in the ODH reaction can be rationalized on the basis of a fast regeneration process, which prevents the structural dynamics from being resolved by the *operando* Raman experiments. While the vanadyl fine structure is resolved for all loadings (see Fig. 4), it is most clearly visible for the 0.57 V/nm² sample. This behavior can be explained by the fact that the MES signals are based on intensity changes triggered by the modulation, which in this context is the conversion of propane. As can be seen in Fig. 4a, the 0.57 V/nm² sample shows a distinct signature for each gas phase. For constant oxygen and pulsed propane flow, the PSD spectrum is dominated by four peaks, at 1004, 1015, 1028, and 1039 cm^{-1}, that coincide with monomeric, dimeric, tetrameric, and pentameric vanadia species, respectively, consistent with the Raman results (see Fig. 2e).

Comparison of the different gas phases, i.e., constant oxygen/pulsed propane to constant propane/pulsed oxygen reveals significant shifts in the peak positions. Interestingly, for all three samples, peaks at around 997, 1005, 1020, 1040, and 1045 cm^{-1} are observed. A vanadyl peak at 997 cm^{-1} is typically associated with crystalline V_2O_5, which is expected at high vanadium loadings. Based on the characterization data, including the visible Raman data discussed above, the presence of crystalline V_2O_5 can be safely ruled out. Furthermore, the peak at 997 cm^{-1} decreases in intensity with increasing vanadium loading, contradicting the current knowledge about V_2O_5 formation on supported VO_x systems.[36–38,42] Since the constant propane mode leads to more reducing conditions, the formation of reduced states appears to be a reasonable explanation. To this end, the reduction of the ceria support may lead to the creation of surface oxygen vacancies, which can subsequently be occupied by vanadia monomers through structural relaxation. Other reasons for the red-shift, such as the binding of water to the vanadyl bond, that were previously described[26] seem unlikely due to the high temperature at which the reaction takes place. Therefore, it is proposed that the unique interaction between surface oxygen vacancies and monomeric species induces a vanadyl red-shift. This interaction is only observed for monomeric species, as described in previous DFT studies.[32] Such a red-shift of monomers was also observed in our preliminary DFT calculations on defective

ceria loaded with monomeric VO_x in the form of VO and VO_2 clusters.[31,32] Such a scenario would also be in good agreement with the changes in the Ce-OH region (see Fig. 3a), where, with increasing vanadium loading, Ce-OH groups are formed close to surface vacancies, indicating that hydrogen from propane is first transferred to VO_x and then to a nearby ceria lattice oxygen before subsequent reaction to water accompanied by the formation of a surface vacancy (see below), located in proximity to a vanadia species. While ceria keeps vanadium in oxidation state +V, the time resolution of MES is sufficient to detect the brief phase in which vanadia is reduced by the reaction before it is quickly re-oxidized by ceria.

Comparison of spectra recorded in constant oxygen (blue) and constant propane (red) mode reveals that monomeric, dimeric, tetrameric, and pentameric vanadia structures are present for both gas phases, confirming that all of those species are active during the ODH reaction, whereas the trimeric vanadia species is only observable in constant oxygen mode, which is likely to also show observer species for the same reasons as mentioned above and described in detail in the SI (see Fig. S18). This makes it likely that trimeric species do not participate in the ODH of propane, which would be consistent with previous DFT results,[32] which have identified trimers as the energetically most stable species on a ceria surface. Therefore, the trimeric species seems to undergo an initial reduction step, which makes it detectable in the constant oxygen mode, but does not continue to react further towards propylene from this reduced state, which leads to its absence in the spectrum in the constant propane mode and the presence of a permanently reduced trimeric species, explaining the observed d-d transitions from the *operando* UV-Vis spectra (see Fig. 2d).

To distinguish the roles of the remaining dimeric, tetrameric, and pentameric species, the vanadyl region of the isotopic MES data is considered (see Fig. 4 b-c and S22, green). In these spectra, only the V=O peaks at 1015 and 1040 cm^{-1} for the 0.57 V/nm² and 1.36 V/nm² samples and the V=O peak at ~1040 cm^{-1} for the 2.83 V/nm² sample are clearly observable, indicating that dimeric and (with higher loading increasingly) pentameric vanadia species are involved in the reaction. A broad signal at the trimeric position is also present, which is in agreement with the aforementioned discussion about the reduced trimeric state. Interestingly, comparison of the blue and red spectra reveals that the V=O peaks of the dimeric and oligomeric species show blue-shifts under more reducing conditions. While DFT calculations of surface vanadia species under such transient conditions are not available in the

literature, the detected spectral behavior may be explained by structural changes in vanadia upon hydrogen abstraction, which is, for example, induced by oxygen vacancies, hydrogen bound to the ceria surface, or V=O - - - H formation. No complete relaxation into nearby vacancies as for monomeric species is observed for dimers and oligomers, probably due to the structural constraints of vanadia chains. The detected blue-shifts in the transient spectra rather imply more condensed vanadia structures, which are subject to increased dipole coupling between neighboring V=O groups.[31,32] Bond-length changes of the vanadyl group, explaining the blue-shift, depending on its interaction with propane/hydrogen atoms and its chemical surroundings, were also previously predicted on silica using DFT calculations.[71] Furthermore, it has already been shown by DFT calculations[32] that for monomeric structures hydrogen that was abstracted to the ceria surface can form hydrogen bonds with V-O-Ce interface oxygen, which may introduce changes in vanadia bond lengths and which may also be possible for dimeric and oligomeric species. Since oxygen vacancies are preferably formed in proximity to vanadia, and hydrogen that is transferred from a V=O bond to the ceria surface is also in close proximity to vanadia (thereby creating hydrogen bonds), only vanadia species that actively participate in the ODH reaction should be subject to such ceria- and/or interface-induced structural changes.[32] Therefore, dimeric and oligomeric vanadia can be identified as key structures for hydrogen abstraction from propane towards the ceria surface. These effects can only be observed using transient spectroscopy, as vanadia is regenerated very fast to oxidation state +V by ceria, making the detection of those species impossible with static spectroscopies. For the samples with higher loadings, the vanadia surface species are shifted towards higher nuclearities. For example, for the 2.83 V/nm² sample, mostly the oligomeric species is detected, which can be explained by the relatively smaller proportion of species with lower nuclearity as well as the even smaller propane conversion of the 2.83 V/nm² sample, both of which decrease the intensity of those contributions below the detection limit of MES. In summary, different vanadia nuclearities fulfill different roles during propane ODH, which leads to different spectroscopic behavior, where different species might red-shift, blue-shift, or not change their position in the PSD spectra, depending on their reaction behavior.

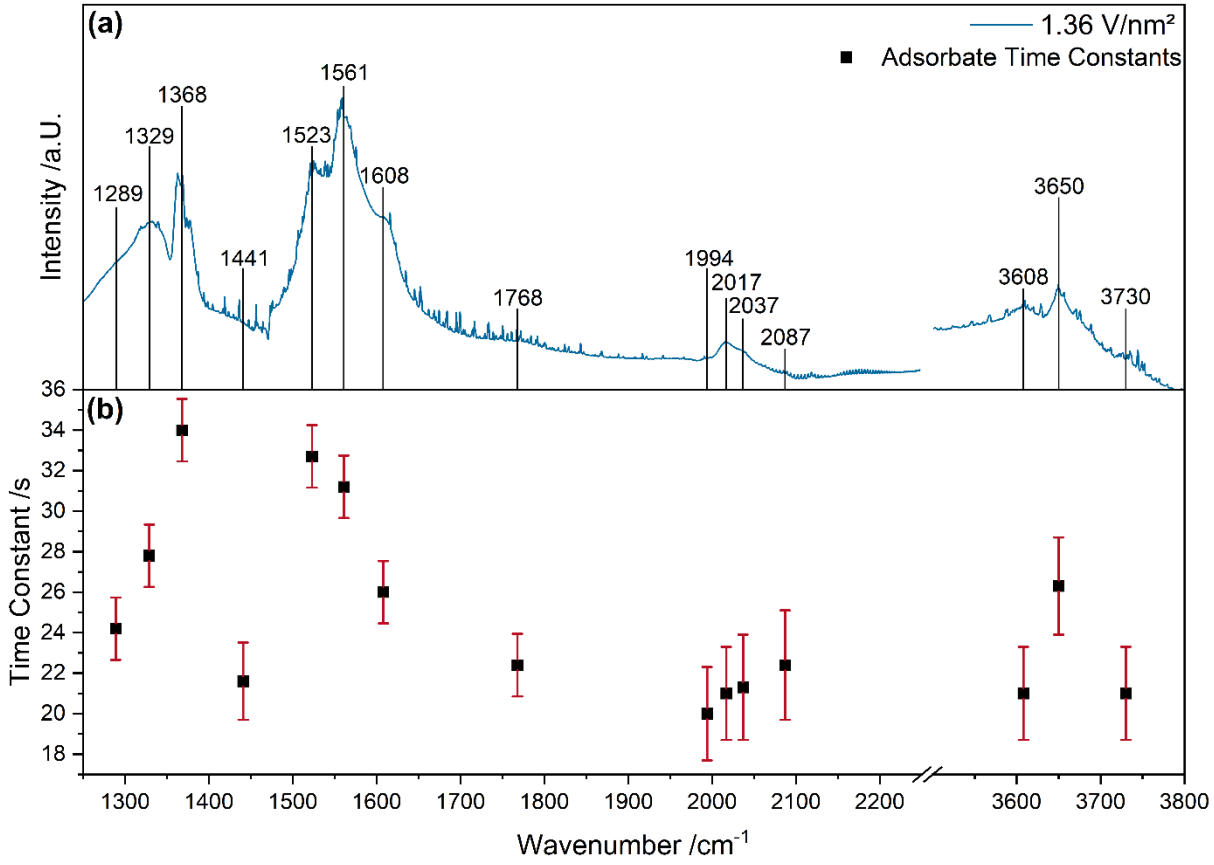

Figure 5: Temporal analysis of propane ODH at 275 °C **(a)** ME-DRIFT spectrum of the 1.36 V/nm² sample during constant propane/pulsed oxygen flow **(b)** Corresponding time constants determined by in-phase angle analysis. Error bars were determined from multiple measurements of the same sample (compare Table S2).

Finally, the time evolution of the surface processes, i.e., the adsorbate dynamics, will be discussed, based on the in-phase angle analysis of the spectra (see experimental section). The top of Fig. 5 depicts the ME-DRIFT spectrum recorded at constant propane/pulsed oxygen flow for the 1.36 V/nm² sample, while the bottom shows the time constants determined for important vibrational features (marked in the top panel), allowing the temporal evolution of the relevant surface processes during the ODH reaction to be visualized. The values of the time constants referring to the 1.36 V/nm² sample are summarized in Table 2, and those for the remaining samples in Table S2.

Table 2*:* Temporal evolution of IR modes involved in propane ODH at 275 °C (example result for the 1.36 V/nm² sample).

Wavenumber /cm^{-1}	Time /s	Assignment
1994	20 ± 2.3	V=O overtone
2017	21 ± 2.3	V=O overtone
3608	21 ± 2.3	V-O-H
3730	21 ± 2.3	Ce-OH I-A
2037	21.3 ± 2.6	V=O overtone
1441	21.6 ± 1.54	υ_s O-C-O
1768	22.4 ± 1.54	υ C=O
2087	22.4 ± 2.7	V=O overtone
1289	24.2 ± 1.54	υ_s C-O
1608	26 ± 1.54	υ_{as} C=C
3650	26.3 ± 2.4	Ce-OH II-B
1329	27.8 ± 1.54	υ C-H
1561	31.2 ± 1.54	υ_{as} COO
1523	32.7 ± 1.54	υ_{as} COO
1368	34 ± 1.54	υ_s CH_3

From the values of the time constants, it can be seen that vanadyl signals, Ce-OH signals from singly bound hydroxyl groups, and V-OH signal groups are the first to be detected. For the following discussion, only the time constant of the overtone will be considered, which is explained in the SI (see Fig. S5). As there is no evidence from static *operando* spectroscopic for the permanent reduction of vanadia, but only from transient results, V-O-H formation is likely to occur very fast and to be followed by a hydrogen transfer to the ceria surface, thereby regenerating the vanadia structure.[33] Such a scenario is supported by DFT results, which propose the reduction of ceria lattice oxygen to be energetically more favorable than vanadia reduction.[31–34,39] Continuing with the discussion of Fig. 3a, within the time frame of the initial processes, also the feature at ~1440 cm^{-1} (O-C-O) appears. The temporal evolution suggests that the corresponding adsorbate represents the state in which propane is initially adsorbed, either during or after the first hydrogen abstraction. In parallel to the 1440 cm^{-1} feature, the peak at ~1780 cm^{-1} is detected, which is correlated with CO_2 formation,[51,52] indicating that CO_2 formation may occur in parallel to propylene formation and not exclusively as a follow-up reaction to propylene formation, as suggested in the literature. Such a scenario is supported by the fact that, with increasing vanadium loading, the peak at 1780 cm^{-1} declines whereas the 1440 cm^{-1} feature stays largely constant, resembling the CO_x and propylene yields, respectively.

The observed behavior supports the proposal of two distinct reaction pathways: one, which proceeds close to vanadia structures, leading mostly to propylene and one, which proceeds on the CeO_2 surface, yielding mostly CO_2. This also explains the smaller increases in selectivity upon doubling the vanadium loading, as 3D structures begin to form and the CO_x pathway is still accessible on the remaining ceria surface. These processes occur in addition to the observed interaction between vanadia monomers and oxygen vacancies. In this context, it seems likely that the blockage of vacancies by vanadia monomers might not only slow down the ceria lattice oxygen dynamics but also block the sites on the ceria surface that play an important role in the reaction pathway towards CO_x, further increasing the complexity of interactions between vanadia, ceria, and propane. Based on the MES data, the two different routes towards CO_2 and propylene, as well as the further reaction of the abstracted hydrogen, can be followed separately. We start with the abstracted hydrogen, which is first transferred to the V=O group and then to the ceria surface, forming singly bound Ce-OH (I-A) and continuing to react towards bridged hydroxyl (II-B) close to an oxygen surface vacancy.[41,70] While no additional signals for this route are observed, it stands to reason that bridged hydroxyls recombine to form singly bound Ce-OH_2 and finally water on a time scale not accessible by MES.[33] For the route towards CO_2 the first adsorption state is followed by structures characterized by features at 1289 cm^{-1} (C-O) and finally 1523 and 1561 cm^{-1} (COO). These were assigned by their late appearance in the temporal evolution as well as their high oxygen content, which is commonly associated with carbonate formation. The latter features are among the last to be detected and exhibit comparably high intensities, indicating that they represent important intermediates towards CO_2 formation.

For the propylene route, after the initial adsorption state, the appearance of the features at 1608 (C=C) and 1329 cm^{-1} (C-H) is in good agreement with a propylene-like intermediate state. In fact, the double bond at 1608 cm^{-1} was previously described in the context of an acrylic coordination of propane.[51] Besides, the peak intensities of the features at 1608 and 1329 cm^{-1} are in agreement with the observed propylene selectivities. The feature at 1368 cm^{-1} (CH_3), which is observed last in the temporal analysis, is likely to originate from the CH_3 group of propylene, which is either adsorbed or about to be desorbed. Based on the detailed mechanistic insights discussed above, we propose a reaction mechanism for propane ODH over VO_x/CeO_2 catalysts (see

Fig.6) containing two pathways, one that occurs close to vanadia and leads to propylene, and one that occurs on ceria and leads to CO_x.

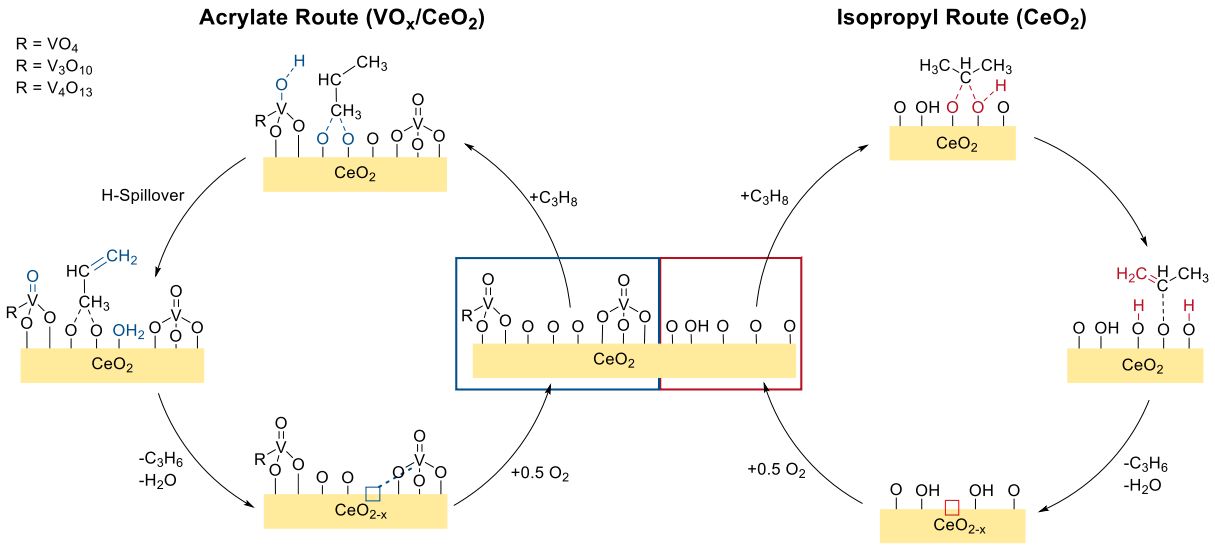

Figure 6: Proposed reaction mechanism for propane ODH over VO_x/CeO_2 catalysts. As shown on the left, in the vicinity of surface vanadia, the reaction proceeds via an acrylate intermediate. On ceria (i.e. at a large distance from surface vanadia), the reaction is proposed to proceed via an isopropyl intermediate (on the right).

4. Conclusion

We present the first application of conventional *operando* spectroscopies, ME-DRIFTS, and isotopic ME-DRIFTS to ODH reactions of alkanes, focusing on the mechanistic investigation of propane ODH, which is of great interest for commercial applications. Previously established, commonly applied *operando* spectroscopy provides significant insights into the reaction mechanism, however, the surface dynamics and the role of vanadia have not been clarified yet.[27] By applying modulation excitation spectroscopy in combination with multiple *operando* spectroscopies, we were able to greatly enhance the level of understanding of propane ODH over supported vanadia catalysts.

We were able to demonstrate that ceria actively participates in the reaction, providing surface oxygen for the oxidation of propane and acting as an oxygen buffer with the possibility of reoxidizing the surface via bulk oxygen, mainly producing CO_x. The introduction of vanadia leads to multiple interactions, which change the activity of the catalyst. First, monomeric vanadia species are shown to slow down the oxygen dynamics in the catalyst by irreversibly blocking surface vacancies required for CO_x production, resulting in a decreased conversion and CO_x production. The addition of vanadia enables a second reaction pathway, which leads to the formation of propylene. The route to CO_x passes through an isopropylic structure on ceria, whereas propylene is formed from an acrylic structure strongly facilitated by proximity to vanadia. Both routes proceed in parallel but at different locations on the surface.

For vanadia-loaded catalysts, the specific role of different vanadia nuclearities for the reaction mechanism was elucidated, i.e., monomeric species block oxygen vacancies, the V=O bonds of dimeric and oligomeric species are involved in the initial hydrogen abstraction, while trimers were too stable for active participation. Hydrogen is then transferred to the ceria surface, regenerating V^{5+} and forming Ce-OH on a very fast time scale, before leading to water and oxygen vacancy formation. These vanadia dynamics were accessible for the first time by MES on VO_x/CeO_2 due to the detected vanadyl fine structure, which allows the structural changes in the vanadia species to be temporally resolved. The observed structural changes shed new light on the role of vanadia in ODH reactions, which both experimentally and theoretically has been proposed to stay in +5 oxidation state during propane ODH over ceria-based catalysts.[3,29–39]

Based on our findings,[27] we propose a detailed reaction mechanism for the ODH of propane over VO_x/CeO_2, directly linking the catalytic activity to solid-state properties (including defects), adsorbate structures, and the roles of different vanadia nuclearities. Our results highlight the potential of (isotopic) modulation excitation IR spectroscopy for elucidating the surface dynamics of propane ODH over supported vanadia. The combination of IR-MES with *operando* spectroscopies provides a powerful methodical approach readily applicable to other catalysts and reactions in the context of oxidation catalysis. Due to the importance of IR spectroscopy in catalysis, we expect widespread adoption of the MES approach for performing detailed mechanistic investigations and for resolving the catalysts' dynamics.

Acknowledgements

The authors acknowledge Dr. Martin Brodrecht for performing nitrogen-adsorption experiments, Dr. Kathrin Hofmann for XRD analysis, and Karl Kopp for technical support. This work was supported by the Deutsche Forschungsgemeinschaft (DFG, HE 4515/11-1) and by a scholarship from the Fonds der Chemischen Industrie im Verband der Chemischen Industrie e.V. (JW).

Supporting Information

Information on the experimental setup; additional data on sample characterization and reactivity behavior; additional *operando* data (DRIFTS, UV-Vis, Raman); additional ME-DRIFTS data, PSD spectra, and temporal analysis.

References

(1) Amghizar, I.; Vandewalle, L. A.; van Geem, K. M.; Marin, G. B. New Trends in Olefin Production. *Engineering* **2017**, *3* (2), 171–178. DOI: 10.1016/J.ENG.2017.02.006.

(2) Cavani, F.; Ballarini, N.; Cericola, A. Oxidative dehydrogenation of ethane and propane: How far from commercial implementation? *Catal. Today* **2007**, *127* (1-4), 113–131. DOI: 10.1016/j.cattod.2007.05.009.

(3) Carrero, C. A.; Schloegl, R.; Wachs, I. E.; Schomaecker, R. Critical Literature Review of the Kinetics for the Oxidative Dehydrogenation of Propane over Well-Defined Supported Vanadium Oxide Catalysts. *ACS Catal.* **2014**, *4* (10), 3357–3380. DOI: 10.1021/cs5003417.

(4) Chen, K.; Bell, A. T.; Iglesia, E. Kinetics and Mechanism of Oxidative Dehydrogenation of Propane on Vanadium, Molybdenum, and Tungsten Oxides. *J. Phys. Chem. B* **2000**, *104* (6), 1292–1299. DOI: 10.1021/jp9933875.

(5) Kim, H.; Kosuda, K. M.; van Duyne, R. P.; Stair, P. C. Resonance Raman and surface- and tip-enhanced Raman spectroscopy methods to study solid catalysts and heterogeneous catalytic reactions. *Chem. Soc. Rev.* **2010**, *39* (12), 4820–4844. DOI: 10.1039/c0cs00044b. Published Online: Oct. 19, 2010.

(6) Zabilska, A.; Clark, A. H.; Moskowitz, B. M.; Wachs, I. E.; Kakiuchi, Y.; Copéret, C.; Nachtegaal, M.; Kröcher, O.; Safonova, O. V. Redox Dynamics of Active VO x Sites Promoted by TiO x during Oxidative Dehydrogenation of Ethanol Detected by Operando Quick XAS. *JACS Au* **2022**, *2* (3), 762–776. DOI: 10.1021/jacsau.2c00027. Published Online: Mar. 14, 2022.

(7) Chiarello, G. L.; Lu, Y.; Agote-Arán, M.; Pellegrini, R.; Ferri, D. Changes of Pd Oxidation State in Pd/Al_2O_3 Catalysts Using Modulated Excitation DRIFTS. *Catalysts* **2021**, *11* (1), 116. DOI: 10.3390/catal11010116.

(8) Vecchietti, J.; Bonivardi, A. L.; Xu, W.; Stacchiola, D.; Delgado, J. J.; Calatayud, M.; Collins, S. E. Understanding the Role of Oxygen Vacancies in the Water Gas Shift Reaction on Ceria-Supported Platinum Catalysts. *ACS Catal.* **2014** (4), 2088–2096. DOI: 10.1021/cs500323u.

(9) Aguirre, A.; Barrios, C. E.; Aguilar-Tapia, A.; Zanella, R.; Baltanás, M. A.; Collins, S. E. In-Situ DRIFT Study of Au–Ir/Ceria Catalysts: Activity and Stability for CO Oxidation. *Top. Catal.* **2015**, *59* (2-4), 347–356. DOI: 10.1007/s11244-015-0425-6.

(10) Aguirre, A.; Zanella, R.; Barrios, C.; Hernández, S.; Bonivardi, A.; Collins, S. E. Gold Stabilized with Iridium on Ceria–Niobia Catalyst: Activity and Stability for CO Oxidation. *Top. Catal.* **2019**, *62* (12), 977–988. DOI: 10.1007/s11244-019-01185-y.

(11) del Río, E.; Collins, S. E.; Aguirre, A.; Chen, X.; Delgado, J. J.; Calvino, J. J.; Bernal, S. Reversible deactivation of a $Au/Ce_{0.62}Zr_{0.38}O_2$ catalyst in CO oxidation: A systematic study of CO_2-triggered carbonate inhibition. *J. Catal.* **2014**, *316*, 210–218. DOI: 10.1016/j.jcat.2014.05.016.

(12) Fernández-García, S.; Collins, S. E.; Tinoco, M.; Hungría, A. B.; Calvino, J. J.; Cauqui, M. A.; Chen, X. Influence of {111} nanofaceting on the dynamics of CO adsorption and oxidation over Au supported on CeO_2 nanocubes: An operando DRIFT insight. *Catal. Today* **2019**, *336*, 90–98. DOI: 10.1016/j.cattod.2019.01.078.

(13) Ferri, D.; Newton, M. A.; Di Michiel, M.; Chiarello, G. L.; Yoon, S.; Lu, Y.; Andrieux, J. Revealing the Dynamic Structure of Complex Solid Catalysts Using Modulated Excitation X-ray Diffraction. *Angew. Chem. Int. Ed.* **2014**, *126* (34), 9036–9040. DOI: 10.1002/ange.201403094.

(14) Weyel, J.; Ziemba, M.; Hess, C. Elucidating Active CO–Au Species on $Au/CeO_2(111)$: A Combined Modulation Excitation DRIFTS and Density Functional Theory Study. *Top. Catal.* **2022.** DOI: 10.1007/s11244-022-01599-1.

(15) Greenaway, A. G.; Marberger, A.; Thetford, A.; Lezcano-González, I.; Agote-Arán, M.; Nachtegaal, M.; Ferri, D.; Kröcher, O.; Catlow, C. R. A.; Beale, A. M. Detection of key transient Cu intermediates in SSZ-13 during NH_3 -SCR deNO_x by modulation excitation IR spectroscopy. *Chem. Sci.* **2020**, *11* (2), 447–455. DOI: 10.1039/C9SC04905C.

(16) Nuguid, R. J. G.; Ferri, D.; Kröcher, O. Design of a Reactor Cell for Modulated Excitation Raman and Diffuse Reflectance Studies of Selective Catalytic Reduction Catalysts. *Emiss. Control Sci. Technol.* **2019**, *5* (4), 307–316. DOI: 10.1007/s40825-019-00141-2.

(17) Nuguid, R. J. G.; Ferri, D.; Marberger, A.; Nachtegaal, M.; Kröcher, O. Modulated Excitation Raman Spectroscopy of V_2O_5/TiO_2: Mechanistic Insights into the Selective Catalytic Reduction of NO with NH_3. *ACS Catal.* **2019**, *9* (8), 6814–6820. DOI: 10.1021/acscatal.9b01514.

(18) Aguirre, A.; Collins, S. E. Selective detection of reaction intermediates using concentration-modulation excitation DRIFT spectroscopy. *Catal. Today* **2013**, *205*, 34–40. DOI: 10.1016/j.cattod.2012.08.020.

(19) Hemmingsson, F.; Schaefer, A.; Skoglundh, M.; Carlsson, P.-A. CO_2 Methanation over Rh/CeO_2 Studied with Infrared Modulation Excitation Spectroscopy and Phase Sensitive Detection. *Catalysts* **2020**, *10* (6), 601. DOI: 10.3390/catal10060601.

(20) König, C. F.J.; Schildhauer, T. J.; Nachtegaal, M. Methane Synthesis and Sulfur Removal over a Ru Catalyst Probed In Situ with High Sensitivity X-Ray Absorption Spectroscopy. *J. Catal.* **2013**, *305*, 92–100. DOI: 10.1016/j.jcat.2013.05.002.

(21) Serrer, M.-A.; Gaur, A.; Jelic, J.; Weber, S.; Fritsch, C.; Clark, A. H.; Saraçi, E.; Studt, F.; Grunwaldt, J.-D. Structural dynamics in Ni–Fe catalysts during CO_2 methanation – role of iron oxide clusters. *Catal. Sci. Technol.* **2020**, *10* (22), 7542–7554. DOI: 10.1039/D0CY01396J.

(22) Delgado, D.; Sanchis, R.; Solsona, B.; Concepción, P.; López Nieto, J. M. Influence of the Nature of the Promoter in NiO Catalysts on the Selectivity to Olefin During the Oxidative Dehydrogenation of Propane and Ethane. *Top. Catal.* **2020**, *63* (19-20), 1731–1742. DOI: 10.1007/s11244-020-01329-5.

(23) Lu, W.-D.; Wang, D.; Zhao, Z.; Song, W.; Li, W.-C.; Lu, A.-H. Supported Boron Oxide Catalysts for Selective and Low-Temperature Oxidative Dehydrogenation of Propane. *ACS Catal.* **2019**, *9* (9), 8263–8270. DOI: 10.1021/acscatal.9b02284.

(24) Daniell, W.; Ponchel, A.; Kuba, S.; Anderle, F.; Weingand, T.; Gregory, D. H.; Knözinger, H. Characterization and Catalytic Behavior of VO_x-CeO_2 Catalysts for the Oxidative Dehydrogenation of Propane. *Top. Catal.* **2002**, *20* (1), 65–74. DOI: 10.1023/A:1016399315511.

(25) Beck, B.; Harth, M.; Hamilton, N. G.; Carrero, C.; Uhlrich, J. J.; Trunschke, A.; Shaikhutdinov, S.; Schubert, H.; Freund, H.-J.; Schlögl, R.; Sauer, J.; Schomäcker, R. Partial oxidation of ethanol on vanadia catalysts on supporting oxides with different

redox properties compared to propane. *J. Catal.* **2012**, *296*, 120–131. DOI: 10.1016/j.jcat.2012.09.008.

(26) Ober, P.; Rogg, S.; Hess, C. Direct Evidence for Active Support Participation in Oxide Catalysis: Multiple Operando Spectroscopy of VO_x/Ceria. *ACS Catal.* **2020**, *10* (5), 2999–3008. DOI: 10.1021/acscatal.9b05174.

(27) Schumacher, L.; Hess, C. The active role of the support in propane ODH over VO_x/CeO_2 catalysts studied using multiple operando spectroscopies. *J. Catal.* **2021**, *398* (13), 29–43. DOI: 10.1016/j.jcat.2021.04.006.

(28) Taylor, M. N.; Carley, A. F.; Davies, T. E.; Taylor, S. H. The Oxidative Dehydrogenation of Propane Using Vanadium Oxide Supported on Nanocrystalline Ceria. *Top. Catal.* **2009**, *52* (12), 1660–1668. DOI: 10.1007/s11244-009-9307-0.

(29) Dinse, A.; Frank, B.; Hess, C.; Habel, D.; Schomäcker, R. Oxidative dehydrogenation of propane over low-loaded vanadia catalysts: Impact of the support material on kinetics and selectivity. *J. Mol. Catal. A: Chemical* **2008**, *289* (1-2), 28–37. DOI: 10.1016/j.molcata.2008.04.007.

(30) Popa, C.; Ganduglia-Pirovano, M. V.; Sauer, J. Periodic Density Functional Theory Study of VO_n Species Supported on the CeO_2 (111) Surface. *J. Phys. Chem. C* **2011**, *115* (15), 7399–7410. DOI: 10.1021/jp108185y.

(31) Penschke, C.; Paier, J.; Sauer, J. Vanadium Oxide Oligomers and Ordered Monolayers Supported on CeO_2 (111): Structure and Stability Studied by Density Functional Theory. *J. Phys. Chem. C* **2018**, *122* (16), 9101–9110. DOI: 10.1021/acs.jpcc.8b01998.

(32) Penschke, C.; Paier, J.; Sauer, J. Oligomeric Vanadium Oxide Species Supported on the CeO_2 (111) Surface: Structure and Reactivity Studied by Density Functional Theory. *J. Phys. Chem. C* **2013**, *117* (10), 5274–5285. DOI: 10.1021/jp400520j.

(33) Huang, C.; Wang, Z.-Q.; Gong, X.-Q. Activity and selectivity of propane oxidative dehydrogenation over VO_3/CeO_2 (111) catalysts: A density functional theory study. *Chin. J. Catal.* **2018**, *39* (9), 1520–1526. DOI: 10.1016/S1872-2067(18)63072-4.

(34) Ganduglia-Pirovano, M. V.; Popa, C.; Sauer, J.; Abbott, H.; Uhl, A.; Baron, M.; Stacchiola, D.; Bondarchuk, O.; Shaikhutdinov, S.; Freund, H.-J. Role of ceria in

oxidative dehydrogenation on supported vanadia catalysts. *J. Am. Chem. Soc.* **2010**, *132* (7), 2345–2349. DOI: 10.1021/ja910574h.

(35) Iglesias-Juez, A.; Martínez-Huerta, M. V.; Rojas-García, E.; Jehng, J.-M.; Bañares, M. A. On the Nature of the Unusual Redox Cycle at the Vanadia Ceria Interface. *J. Phys. Chem. C* **2018**, *122* (2), 1197–1205. DOI: 10.1021/acs.jpcc.7b09832.

(36) Martínez-Huerta, M. V.; Deo, G.; Fierro, J. L. G.; Bañares, M. A. Operando Raman-GC Study on the Structure−Activity Relationships in V^{5+}/CeO_2 Catalyst for Ethane Oxidative Dehydrogenation: The Formation of CeVO 4. *J. Phys. Chem. C* **2008**, *112* (30), 11441–11447. DOI: 10.1021/jp802827t.

(37) Martínez-Huerta, M. Nature of the vanadia-ceria interface in V^{5+}/CeO_2 catalysts and its relevance for the solid-state reaction toward CeVO4 and catalytic properties. *J. Catal.* **2004**, *225* (1), 240–248. DOI: 10.1016/j.jcat.2004.04.005.

(38) Bañares, M.A.; Martínez-Huerta, M.V.; Gao, X.; Fierro, J.L.G.; Wachs, I.E. Dynamic behavior of supported vanadia catalysts in the selective oxidation of ethane. *Catal. Today* **2000**, *61* (1-4), 295–301. DOI: 10.1016/S0920-5861(00)00388-6.

(39) Kropp, T.; Paier, J.; Sauer, J. Support effect in oxide catalysis: methanol oxidation on vanadia/ceria. *J. Am. Chem. Soc.* **2014**, *136* (41), 14616–14625. DOI: 10.1021/ja508657c. Published Online: Oct. 2, 2014.

(40) Wu, Z.; Rondinone, A. J.; Ivanov, I. N.; Overbury, S. H. Structure of Vanadium Oxide Supported on Ceria by Multiwavelength Raman Spectroscopy. *J. Phys. Chem. C* **2011**, *115* (51), 25368–25378. DOI: 10.1021/jp2084605.

(41) Filtschew, A.; Hofmann, K.; Hess, C. Ceria and Its Defect Structure: New Insights from a Combined Spectroscopic Approach. *J. Phys. Chem. C* **2016**, *120* (12), 6694–6703. DOI: 10.1021/acs.jpcc.6b00959.

(42) Waleska, P. S.; Hess, C. Oligomerization of Supported Vanadia: Structural Insight Using Surface-Science Models with Chemical Complexity. *J. Phys. Chem. C* **2016**, *120* (33), 18510–18519. DOI: 10.1021/acs.jpcc.6b01672.

(43) Ziemba, M.; Weyel, J.; Hess, C. Elucidating the mechanism of the reverse water–gas shift reaction over Au/CeO_2 catalysts using operando and transient

spectroscopies. *Appl. Catal. B: Environmental* **2022**, *301*, 120825. DOI: 10.1016/j.apcatb.2021.120825.

(44) Schilling, C.; Hofmann, A.; Hess, C.; Ganduglia-Pirovano, M. V. Raman Spectra of Polycrystalline CeO_2 : A Density Functional Theory Study. *J. Phys. Chem. C* **2017**, *121* (38), 20834–20849. DOI: 10.1021/acs.jpcc.7b06643.

(45) Schilling, C.; Ziemba, M.; Hess, C.; Ganduglia-Pirovano, M. V. Identification of single-atom active sites in CO oxidation over oxide-supported Au catalysts. *J. Catal.* **2020**, *383* (85), 264–272. DOI: 10.1016/j.jcat.2020.01.022.

(46) Dieter Baurecht; Urs Peter Fringeli. Quantitative modulated excitation Fourier transform infrared spectroscopy. *Rev. Sci. Instr.* **2001**, *72* (10), 3782. DOI: 10.1063/1.1400152.

(47) Zenodo, https://zenodo.org/record/3613876#.YtAxLBxCSUk, Weyel, J. *Phase Sensitive Detection for Spectroscopy*; 2020. DOI: 10.5281/zenodo.3613876 (accessed 2022-07-14).

(48) Yu, T.; Lim, B.; Xia, Y. Aqueous-Phase Synthesis of Single-Crystal Ceria Nanosheets. *Angew. Chem. Int. Ed.* **2010**, *122* (26), 4586–4589. DOI: 10.1002/ange.201001521.

(49) Hess, C. New advances in using Raman spectroscopy for the characterization of catalysts and catalytic reactions. *Chem. Soc. Rev.* **2021**, *50* (5), 3519–3564. DOI: 10.1039/d0cs01059f.

(50) Baron, M.; Abbott, H.; Bondarchuk, O.; Stacchiola, D.; Uhl, A.; Shaikhutdinov, S.; Freund, H.-J.; Popa, C.; Ganduglia-Pirovano, M. V.; Sauer, J. Resolving the Atomic Structure of Vanadia Monolayer Catalysts: Monomers, Trimers, and Oligomers on Ceria. *Angew. Chem. Int. Ed.* **2009**, *121* (43), 8150–8153. DOI: 10.1002/ange.200903085.

(51) Hu, Z.; Wang, Z.; Guo, Y.; Wang, L.; Guo, Y.; Zhang, J.; Zhan, W. Total Oxidation of Propane over a Ru/CeO_2 Catalyst at Low Temperature. *Environ. Sci. Technol.* **2018**, *52* (16), 9531–9541. DOI: 10.1021/acs.est.8b03448. Published Online: Aug. 2, 2018.

(52) Wang, H.; Zhou, H.; Li, S.; Ge, X.; Wang, L.; Jin, Z.; Wang, C.; Ma, J.; Chu, X.; Meng, X.; Zhang, W.; Xiao, F.-S. Strong Oxide–Support Interactions Accelerate

Selective Dehydrogenation of Propane by Modulating the Surface Oxygen. *ACS Catal.* **2020**, *10* (18), 10559–10569. DOI: 10.1021/acscatal.0c02782.

(53) Davydov, A. Surface complexes of propylene and their role in catalytic oxidation. *J. Catal.* **1978**, *55* (3), 299–313. DOI: 10.1016/0021-9517(78)90218-X.

(54) Wang, Y.; Li, D.; Li, K.; Farrauto, R. Enhanced propane and carbon monoxide oxidation activity by structural interactions of CeO_2 with MnO_x/Nb_2O_{5-x} catalysts. *Appl. Catal. B: Environmental* **2020**, *267* (5), 118363. DOI: 10.1016/j.apcatb.2019.118363.

(55) Wang, B.; Wu, X.; Ran, R.; Si, Z.; Weng, D. IR characterization of propane oxidation on $Pt/CeO_2–ZrO_2$: The reaction mechanism and the role of Pt. *J. Mol. Catal. A: Chemical* **2012**, *356*, 100–105. DOI: 10.1016/j.molcata.2011.12.030.

(56) Huang, B.; Gillen, R.; Robertson, J. Study of CeO 2 and Its Native Defects by Density Functional Theory with Repulsive Potential. *J. Phys. Chem. C* **2014**, *118* (42), 24248–24256. DOI: 10.1021/jp506625h.

(57) Nitsche, D.; Hess, C. Structure of Isolated Vanadia and Titania: A Deep UV Raman, UV–Vis, and IR Spectroscopic Study. *J. Phys. Chem. C* **2016**, *120* (2), 1025–1037. DOI: 10.1021/acs.jpcc.5b10317.

(58) Skorodumova, N. V.; Ahuja, R.; Simak, S. I.; Abrikosov, I. A.; Johansson, B.; Lundqvist, B. I. Electronic, bonding, and optical properties of CeO_2 and Ce_2O_3 from first principles. *Phys. Rev. B* **2001**, *64* (11), 115108. DOI: 10.1103/PhysRevB.64.115108.

(59) Liu, J.; Zhao, Z.; Xu, C.; Duan, A.; Jiang, G. CeO_2-supported vanadium oxide catalysts for soot oxidation: the roles of molecular structure and nanometer effect. *J. Rare Earths* **2010**, *28* (2), 198–204. DOI: 10.1016/S1002-0721(09)60080-6.

(60) Deeth, R. J. Electronic structures and d-d spectra of vanadium(IV) and VO^{2+} complexes: discrete variational Xα calculations. *J. Chem. Soc., Dalton Trans.* **1991** (6), 1467–1477. DOI: 10.1039/DT9910001467.

(61) Waleska, P.; Rupp, S.; Hess, C. Operando Multiwavelength and Time-Resolved Raman Spectroscopy: Structural Dynamics of a Supported Vanadia Catalyst at Work. *J. Phys. Chem. C* **2018**, *122* (6), 3386–3400. DOI: 10.1021/acs.jpcc.7b10518.

(62) Rogg, S.; Hess, C. CO_2 as a soft oxidant for propane oxidative dehydrogenation: A mechanistic study using operando UV Raman spectroscopy. *J. CO2 Util.* **2021**, *50*, 101604. DOI: 10.1016/j.jcou.2021.101604.

(63) Schilling, C.; Hess, C. Real-Time Observation of the Defect Dynamics in Working Au/CeO_2 Catalysts by Combined Operando Raman/UV–Vis Spectroscopy. *J. Phys. Chem. C* **2018**, *122* (5), 2909–2917. DOI: 10.1021/acs.jpcc.8b00027.

(64) Li, Y.; Wei, Z.; Gao, F.; Kovarik, L.; Baylon, R. A. L.; Peden, C. H. F.; Wang, Y. Effect of Oxygen Defects on the Catalytic Performance of VO_x/CeO_2 Catalysts for Oxidative Dehydrogenation of Methanol. *ACS Catal.* **2015**, *5* (5), 3006–3012. DOI: 10.1021/cs502084g.

(65) Hasan, M. A.; Zaki, M. I.; Pasupulety, L. IR Investigation of the Oxidation of Propane and Likely C_3 and C_2 Products over Group IVB Metal Oxide Catalysts. *J. Phys. Chem. B* **2002**, *106* (49), 12747–12756. DOI: 10.1021/jp0214413.

(66) Pokrovski, K.; Jung, K. T. Investigation of CO and CO_2 Adsorption on Tetragonal and Monoclinic Zirconia. *Langmuir* **2001**, *17* (14), 4297–4303. DOI: 10.1021/la001723z.

(67) Li, C.; Sakata, Y.; Arai, T.; Domen, K.; Maruya, K.-i.; Onishi, T. Carbon monoxide and carbon dioxide adsorption on cerium oxide studied by Fourier-transform infrared spectroscopy. Part 1.—Formation of carbonate species on dehydroxylated CeO_2, at room temperature. *J. Chem. Soc., Faraday Trans. 1* **1989**, *85* (4), 929. DOI: 10.1039/f19898500929.

(68) Burcham, L. J.; Deo, G.; Gao, X.; Wachs, I. E. In-Situ IR, Raman, and UV-Vis DRS Spectroscopy of Supported Vanadium Oxide Catalysts During Methanol Oxidation. *Top. Catal.* **2000**, *11/12* (1/4), 85–100. DOI: 10.1023/A:1027275225668.

(69) Sambeth, J. E.; Centeno, M. A.; Paúl, A.; Briand, L. E.; Thomas, H. J.; Odriozola, J. A. In situ DRIFTS study of the adsorption–oxidation of CH_3OH on V_2O_5. *J. Mol. Catal. A: Chemical* **2000**, *161* (1-2), 89–97. DOI: 10.1016/S1381-1169(00)00152-7.

(70) Badri, A.; Binet, C.; Lavalley, J.-C. An FTIR study of surface ceria hydroxy groups during a redox process with H_2. *Faraday Trans.* **1996**, *92* (23), 4669. DOI: 10.1039/ft9969204669.

(71) Rozanska, X.; Fortrie, R.; Sauer, J. Oxidative Dehydrogenation of Propane by Monomeric Vanadium Oxide Sites on Silica Support. *J. Phys. Chem. C* **2007**, *111* (16), 6041–6050. DOI: 10.1021/jp071409e.